Dynamics of the optical Freedericksz transition

F. Marquis,* P. Meystre, and E. M. Wright
Optical Sciences Center, University of Arizona, Tucson, Arizona 85721

A. E. Kaplan†
School of Electrical Engineering, Purdue University, West Lafayette, Indiana 47907

(Received 25 June 1986; revised manuscript received 11 December 1986)

We investigate theoretically dynamical aspects of the optical Freedericksz transition in nematic liquid crystals. Specifically, we analyze (1) the existence and stability of a sequence of higher-order longitudinal modes past the Freedericksz transition, (2) effects due to transverse correlations of the molecular orientation, and (3) the effects of thermal noise on the stability of the spatial modes. Higher-order longitudinal modes are studied both in the weak-anisotropy limit, in which case the problem reduces at steady state to a sine-Gordon equation, and in the general case, using a combination of analytical and numerical methods. They can be excited by the influence of internal fluctuations. Transverse correlations are shown to lead to the existence of transverse inhomogeneities ("kinks") of the direct-angle distribution that can appear even under plane-wave illumination.

I. INTRODUCTION

The optical Freedericksz transition (OFT), i.e., the change in refractive index of a nematic liquid crystal due to the distortion of the director field under the influence of a laser beam, has been the object of considerable studies in the last few years.[1–13] The Freedericksz transition was originally discovered in 1927 by employing a static magnetic field, but its recent observation[1–3] under laser irradiation reawakened the interest in this problem.

In the paper we investigate theoretically the dynamics of nematic liquid crystals illuminated by a laser beam. In particular, we analyze static and dynamical aspects of the OFT related to (1) the existence of further transitions corresponding to higher-order longitudinal modes in the crystal, (2) their stability against small perturbations and noise, and (3) transverse effects due to transverse correlations of the molecular orientation. Higher-order longitudinal configurations are important not only from a basic physics point of view, but also for potential applications, e.g., in spatial light modulation, bistable devices, and nonlinear waveguides. The dynamical study of transverse effects near a phase transition, a problem of obvious practical importance, is also relevant to the general study of nucleation.

This paper is organized as follows: Sec. II defines our model and notation. Section III presents analytical results obtained in a plane-wave, one-dimensional, small-anisotropy model of the OFT. The steady-state characteristics of higher-order longitudinal modes of the director angle are discussed. The steady-state inclusion of transverse effects is given in Sec. IV, where we show that transverse inhomogeneities in the director-angle distribution are then possible, even under plane-wave illumination. Analytical results are derived for simple pump-beam profiles. They are useful in providing intuition for the numerical work of the following sections. Sections V–VII address the dynamics of the liquid crystal. A linear stability analysis of higher-order longitudinal modes presented in Sec. V shows them to be unstable, but with possibly exceedingly long lifetimes. Furthermore, the existence of transversely propagating wave fronts is predicted in the vicinity of the OFT threshold. Section VI gives the main results of a numerical study of the full nonlinear problem. Section VII returns to a one-dimensional model to discuss the effects of internal noise on the stability and accessibility of higher-order spatial modes. Finally, Sec. VIII is a summary and conclusion.

II. MODEL AND NOTATION

We consider a homeotropic nematic liquid crystal of thickness d and infinite transverse dimensions irradiated by a cw laser incident along the z axis perpendicular to its surface, and polarized in the x direction, see Fig. 1. The

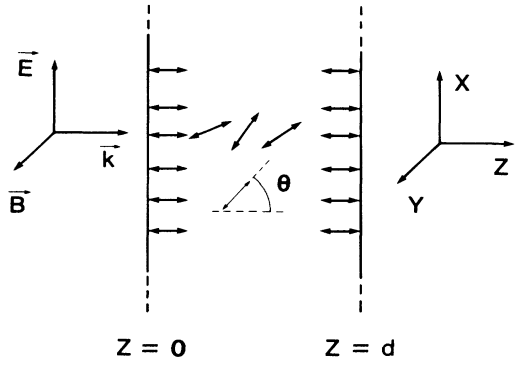

FIG. 1. Sample of nematic liquid crystal, homeotropically aligned, pumped perpendicularly by a linearly polarized laser beam. θ is the angle between the directors and the z axis.

free energy of this system is[14]

$$F=\int_V d^3r\tfrac{1}{2}\{k_{11}(\nabla\cdot\mathbf{n})^2+k_{22}[\mathbf{n}\cdot(\nabla\times\mathbf{n})]^2 +k_{33}(\mathbf{n}\times\nabla\times\mathbf{n})^2+2F_{\rm em}]\} \ . \tag{2.1}$$

Here k_{ii} $(i=1,2,3)$ are the Franck elastic constants of splaying, twisting, and bending, respectively, $\mathbf{n}$ is the director field of the molecules, $\mathbf{n}=(\sin\theta,0,\cos\theta)$, where we assume that the polarization of the field inside the liquid crystal remains in the x-z plane, and $F_{\rm em}$ is the electromagnetic energy density,

$$F_{\rm em}=\tfrac{1}{2}(\mathbf{E}\cdot\mathbf{D}+\mathbf{B}\cdot\mathbf{H}) \ . \tag{2.2}$$

In this paper we take for simplicity all elastic constants to be equal, $k_{11}=k_{22}=k_{33}\equiv\kappa$. Because the magnetic susceptibility is much smaller than the dielectric susceptibility, we assume the liquid crystal to be nonmagnetic. The dielectric tensor $\underline{\epsilon}$ of the medium is a function of the orientation $\theta(z)$ of the director, which in turn is a function of the laser light intensity

$$\mathbf{D}=\underline{\epsilon}(\theta)\mathbf{E} \ , \tag{2.3}$$

where

$$\mathbf{E}(x,y,z,t)=\mathbf{E}(x,y,z)\exp[i(kz-\omega t)]+\text{c.c.} \tag{2.4}$$

is the electric field inside the crystal. It can then be shown[12] that if beam diffraction and absorption are negligible, the z component $S_z(x,y,z)$ of the Poynting vector remains constant as the field propagates along the crystal, $S_z(x,y,z)=S_z(x,y)$. For this preliminary study we further restrict ourselves to one transverse coordinate, so that $S_z(x,y)=S_z(x)$ only. Within the slowly-varying-envelope approximation, (2.2)–(2.4) then yield

$$F_{\rm em}=\frac{S_z(x)n_0}{c}\frac{1}{(1-r\sin^2\theta)^{1/2}} \ , \tag{2.5}$$

where

$$r=1-n_0^2/n_e^2 \ . \tag{2.6}$$

Here n_0 and n_e are the ordinary and extraordinary indexes of refraction of the crystal. Minimizing the free energy (2.1) yields the well-known Euler-Lagrange equation of motion for the director-angle distribution $\theta(x,z)$

$$\partial_{xx}^2\theta+\partial_{zz}^2\theta+\beta(x)r\frac{\sin\theta\cos\theta}{(1-r\sin^2\theta)^{3/2}}=0 \ , \tag{2.7}$$

where

$$\beta(x)=n_0\frac{S_z(x)}{\kappa c} \tag{2.8}$$

is the scaled z component of the Poynting vector.

Equation (2.7) has been studied extensively as a model for the OFT. Durbin *et al.*[4] studied the plane-wave limit of a similar equation in their paper which reported the first experimental observation of the OFT. Zel'dovich *et al.*[2,15] developed a geometrical-optics theory which incorporated transverse effects. Ong[12] has critically discussed both of these models and advanced a self-consistent geometrical-optics approach. We have here adopted Ong's model.

III. PLANE-WAVE SMALL-ANISOTROPY MODEL

In order to gain some insight into the problem at hand, we first restrict our analysis to a plane-wave input laser. In this case, $\beta(x)$ becomes a constant, and a first integration of Eq. (2.7) yields immediately

$$\tfrac{1}{2}(d_z\theta)^2+\beta\frac{1}{(1-r\sin^2\theta)^{1/2}}=C \ , \tag{3.1}$$

where C is a constant of integration.

Consider first what happens if $r\ll 1$, i.e., $n_0\cong n_e$. The square root in Eq. (3.1) can then be expanded to first order, leading to

$$\tfrac{1}{2}(d_z\theta)^2+\beta\left[1+\frac{r}{2}\sin^2\theta\right]=C \ . \tag{3.2}$$

The constant of integration C can be determined by observing that there is always an extremum angle θ_M for which $d_z\theta=0$, so that

$$C=\beta\left[1+\frac{r}{2}\sin^2\theta_M\right] \ . \tag{3.3}$$

The director angle can thus be expressed implicitly in terms of the elliptic integral

$$\int_0^{\theta(z)}\frac{d\theta'}{(1-\mu^2\sin^2\theta')^{1/2}}=\pm\sqrt{\beta r}\,\sin\theta_M z \ , \tag{3.4}$$

where

$$\mu^2=1/\sin^2\theta_M\geq 1 \ . \tag{3.5}$$

The solution of (3.4) are in the form of elliptic functions

$$\theta(z)=\pm\sin^{-1}[(1/\mu)\mathrm{sn}(\sqrt{\beta r}z,1/\mu)] \ . \tag{3.6}$$

For a homeotropic liquid crystal, $\theta(0)=\theta(d)=0$. These boundary conditions indicate the possibility of spatial modes of $\theta(z)$. Specifically, $\theta(d)=0$ implies

$$\sqrt{\beta r}\,d=2mK(1/\mu) \ , \tag{3.7}$$

where m is an integer and

$$K(1/\mu)\equiv\int_0^{\pi/2}\frac{d\theta}{[1-(1/\mu^2)\sin^2\theta]^{1/2}} \tag{3.8}$$

is a tabulated monotonic function of $1/\mu^2$ with $K(0)=\pi/2$. Since $K(1/\mu)\geq\pi/2$, Eq. (3.7) gives the threshold of the successive modes. In particular, the first mode $m=1$ becomes possible for

$$\sqrt{\beta r}\,d>\pi \ , \tag{3.9}$$

which gives the scaled threshold intensity

$$\beta_{\rm th}^1=\pi^2/d^2r \ , \tag{3.10}$$

which is the threshold of the OFT. For intensities $\beta<\beta_{\rm th}^{1}$, the only possible solution is $\theta(z)=0$, i.e., the directors remain unchanged under the influence of the laser. The shorter the medium, the harder it is to reach the OFT. Furthermore, for a given incident intensity, the maximum angle θ_M is larger, the thicker the medium, as is readily seen from Eqs. (3.5) and (3.7) and the fact that $K(1/\mu)$ is a monotonic function of $1/\mu$. This is because the anchoring conditions of a homeotropic liquid crystal $\theta(0)=\theta(d)=0$ are felt more weakly in the bulk of the crystal for thick samples than for thin ones.

Equation (3.7) also gives the threshold intensity of the mth mode as

$$\beta_{\rm th}^{m}=m^2\pi^2/d^2r \ , \tag{3.11}$$

which shows that the required intensity increases quadratically with the order of the mode. This is reasonable since for higher-order modes the maxima in reorientation occur progressively closer to the boundaries, where the molecules are strongly anchored. Note that for a given intensity, the amplitude $\theta(z)$ of reorientation decreases with m.

Figure 2 illustrates the first and second longitudinal modes of the director angle as functions of z for different normalized incident intensities β. The form (3.6) of $\theta(z)$ shows that for intensities close to the threshold value $\beta_{\rm th}^{m}$, the spatial distribution of the director angles is well approximated by $\sin(m\pi z/d)$. For higher intensities, the corresponding elliptic functions flatten in the middle, indicative of a saturation of the director reorientation in the crystal. The stability of these spatial modes is discussed in Sec. V.

We remark that in the small-anisotropy limit, Eq. (2.7) reduces to the sine-Gordon equation (SGE) and is identical in form to the exact equation for a liquid crystal in a homogeneous static magnetic field applied normally to the equilibrium directors.[16] The results of this section therefore apply equally well to this case.

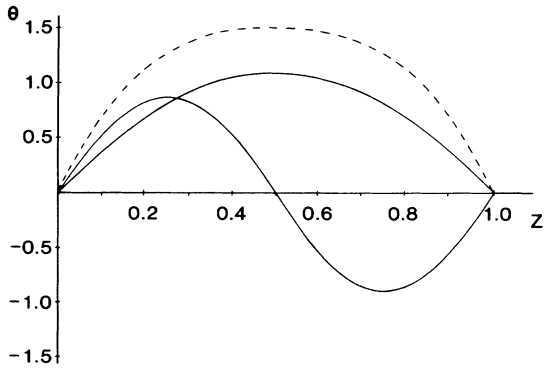

FIG. 2. Reorientation angle distribution θ for the first- and second-order spatial modes as a function of z (in units of d). For the first mode, $\beta=2$ (solid line) and $\beta=6$ (dashed line). For the second mode, $\beta=6$. In all cases, as well as in the following figures, β is scaled to $\beta_{\rm th}^{1}$.

IV. TRANSVERSE EFFECTS–SMALL-REORIENTATION REGIME

So far, our analysis has been limited to the case of plane waves incident on the liquid crystal. This section removes this restriction, and discusses aspects of transverse effects amenable to an analytical solution. A numerical analysis allowing the description of more realistic incident laser beam profiles is presented in Sec. VI. In order to keep the problem tractable, we neglect the effects of diffraction, an approximation valid for thin samples, and limit our analysis to those transverse effects originating in the transverse correlations of the director reorientation. Also, we restrict ourselves in this section to the vicinity of the Freedericksz transition, where the director-angle distribution $\theta(x,z)$ is small enough to justify a third-order expansion. Specifically, we assume [see Eq. (2.7)]

$$\frac{\sin\theta\cos\theta}{(1-r\sin^2\theta)^{3/2}}\cong\theta-\alpha\theta^3 \ , \tag{4.1}$$

where

$$\alpha=\tfrac{2}{3}-3r/2 \ . \tag{4.2}$$

In this limit, Eq. (2.7) can be interpreted as the Euler-Lagrange equation resulting from the Lagrangian density

$$2L=(\partial_x\theta)^2+(\partial_z\theta)^2-\beta r(\theta^2-\alpha\theta^4/2) \ , \tag{4.3}$$

with the variational principle $\delta I=0$, where

$$I=\int dx\int dzL \ . \tag{4.4}$$

A considerable simplification occurs in the vicinity of the OFT, where the z dependence of the problem can be integrated out exactly: The boundary conditions $\theta(x,0)=\theta(x,d)=0$ suggest expanding $\theta(x,z)$ as a Fourier series

$$\theta(x,z)=\sum_{n=1}^{\infty}a_n(x)\sin(n\pi z/d) \ . \tag{4.5}$$

In Sec. III we saw that higher-order spatial modes are absent in the vicinity of the OFT, as they require higher incident intensities. We ignore them here, and restrict the sum (4.5) to its first term[17]

$$\theta(x,z)\cong a(x)\sin(\pi z/d) \ , \tag{4.6}$$

which coincides with the solution (3.6) in the plane-wave small-θ limit. Substituting this ansatz into (4.3) and performing the straightforward integration of the Lagrangian (4.4) over z yields then an Euler-Lagrange equation for $a(x)$ only:

$$d_{xx}^2a+[r\beta(x)(1-3\alpha a^2/4)-\pi^2/d^2]a=0 \ . \tag{4.7}$$

A. Plane-wave illumination

The transverse correlation of the reorientation angle can lead to the appearance of transverse inhomogeneities of $\theta(x,z)$ even under plane-wave illumination. We prove this point by taking the incident laser beam to be a plane wave, $\beta(x)\equiv\beta=$const. Equation (4.7) then becomes

$$d_{xx}^2 a + a(\sigma - \xi a^2) = 0 \ , \tag{4.8}$$

where

$$\sigma = \beta r - \pi^2/d^2 \tag{4.9}$$

and

$$\xi = 3\alpha\beta r/4 \ . \tag{4.10}$$

The homogeneous solutions are easily found by dropping the second-order derivative in Eq. (4.8). For $\sigma > 0$ we readily find the solution $a = 0$ and

$$a_\infty = \pm\sqrt{\sigma/\xi} \ , \tag{4.11}$$

whereas for $\sigma < 0$ only the zero solution applies. This reflects the fact that as the incident intensity β is increased past the threshold $\beta_{\rm th}^1$ of the OFT [compare Eqs. (4.9) and (3.10)], the director angle exhibits a second-order-like phase transition.[12]

The opposite case $\xi < 0$ is characterized by a stable constant solution $a = 0$ for $\sigma < 0$, which becomes metastable at $\sigma = 0$. A third-order expansion is not sufficient to obtain stable solutions past this point, and the next (5th) order in (4.1) must be included. In the remainder of this paper we concentrate on the case $\xi > 0$, $0 < r < \frac{4}{9}$.

In this case a first integration of Eq. (4.8) yields

$$(d_x a)^2 = C - \sigma a^2 + \xi a^4/2 \ , \tag{4.12}$$

where the constant of integration C is given by the asymptotic condition $d_x a(\pm\infty) = 0$, which yields

$$C = \sigma a_\infty^2 - \xi a_\infty^4/2 \ . \tag{4.13}$$

Using Eq. (4.11) to eliminate σ gives

$$d_x a = \pm\sqrt{\xi/2}(a_\infty^2 - a^2) \ , \tag{4.14}$$

whose solutions are ($a_\infty > 0$)

$$a(x) = \pm a_\infty \tanh(a_\infty\sqrt{\xi/2}x + C_1) \tag{4.15}$$

and

$$a(x) = \pm a_\infty \coth(a_\infty\sqrt{\xi/2}x + C_2) \ , \tag{4.16}$$

where C_1 and C_2 are arbitrary constants of integration. The solution (4.16) is clearly unphysical.

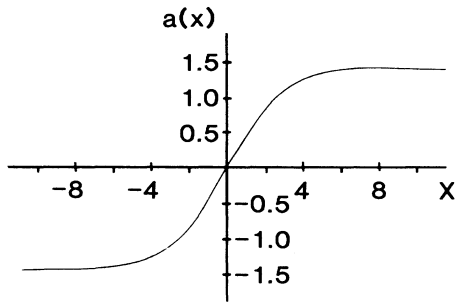

FIG. 3. Inhomogeneous director-angle distribution in the middle of the sample ($z = d/2$) as a function of x for $\beta = 1.2$ and $C_1 = 0$ (arbitrary units). The anisotropy r is fixed in all the figures to $r = 0.23$.

Equation (4.15) indicates that even under plane-wave illumination, the transverse coupling between the molecules of the liquid crystal induces a transverse anisotropy in the reorientation angle θ for sufficiently high incident intensities. The location at which switching between the solutions a_∞ and $-a_\infty$ takes place along the x axis is however undetermined. Similar results have been obtained previously by Brochard[17] for the case of the magnetic Freedericksz transition.

Above threshold, four possible behaviors of the reorientation are thus possible: 3 homogeneous ones, $a = a_\infty$, 0, $-a_\infty$, and the inhomogeneous hyperbolic tangent solution, which is illustrated in Fig. 3.

B. Step-function illumination

Let us now turn to the case of a step-function incident intensity, which also permits an analytical solution and gives an indication of the characteristic transverse dimension over which the OFT diffuses into a region which is below threshold from a region above threshold. Here, the incident scaled intensity distribution is taken as

$$\begin{aligned} \beta(x) &= \beta \quad \text{for } x \geq 0 \\ &= 0 \quad \text{for } x < 0 \ . \end{aligned} \tag{4.17}$$

The parameters σ and ξ in the diffusion equation (4.8) become

$$\begin{aligned} \sigma &= \beta r - \pi^2/d^2 \quad \text{for } x \geq 0 \\ &= -\pi^2/d^2 \quad \text{for } < 0 \ , \end{aligned} \tag{4.18}$$

and

$$\begin{aligned} \xi &= 3\alpha\beta r/4 \quad \text{for } x \geq 0 \\ &= 0 \quad \text{for } x < 0 \ . \end{aligned} \tag{4.19}$$

For $x < 0$, the solution is the exponential

$$a(x) = C_2 \exp(\pi x/d) \ , \tag{4.20}$$

and for $x \geq 0$, it is in the form of the hyperbolic tangent (4.15).

The constants C_1 and C_2 are determined by the continuity of $a(x)$ and of its derivative at $x = 0$. A straightforward calculation gives

$$C_1 = \tanh^{-1}\{(2\sigma)^{-1/2}[-\pi/d + (\pi^2/d^2 + 2\sigma)^{1/2}]\} \ , \tag{4.21}$$

and

$$C_2 = (2\xi)^{-1/2}[-\pi/d + (\pi^2/d^2 + 2\sigma)^{1/2}] \ . \tag{4.22}$$

This general solution is illustrated in Fig. 4. A characteristic transverse diffusion length l_c of the Freedericksz transition may be defined by adding the characteristic lengths of the exponential and hyperbolic tangent. We choose for convenience the characteristic length to be x_c for an exponential of the form $\exp(-x/x_c)$, and x_0 for $\tanh(x/x_0 + a)$. In our case this gives

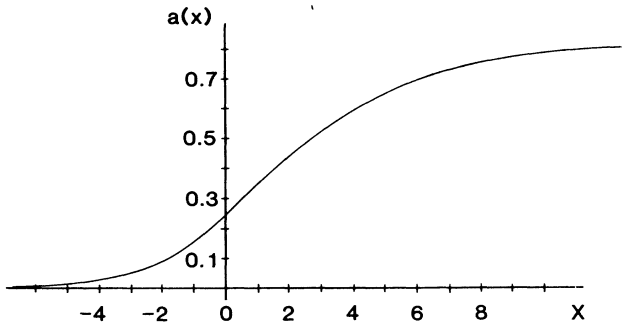

FIG. 4. Transverse distribution $\theta(x)$ at $z=d/2$ for the case of a step-function illumination. Same parameters as in Fig. 3.

$$l_c = x_c + x_0 = d/\pi + \sqrt{2/\sigma}$$

$$= d/\pi + \left[\frac{2}{r(\beta - \pi^2/d^2 r)}\right]^{1/2}$$

$$= \frac{1}{\sqrt{r\beta_{\text{th}}}} + \left[\frac{2}{r(\beta - \beta_{\text{th}})}\right]^{1/2} . \quad (4.23)$$

Figure 5 illustrates the behavior of l_c as a function of the incident intensity S for three values of d. The divergence of the characteristic length around the threshold value is indicative of a second-order phase transition, near the threshold all transverse spatial frequencies are important.

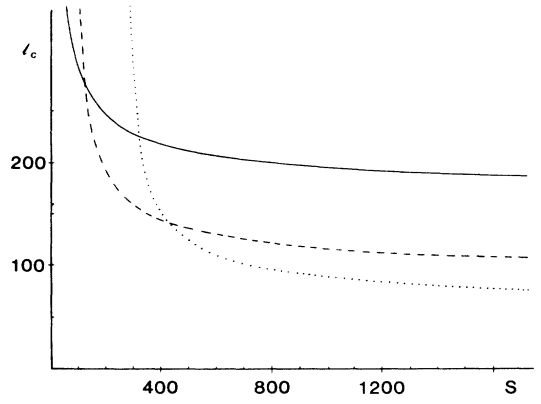

FIG. 5. Transverse diffusion length l_c (μm) of the Freedericksz transition under step-function illumination, as a function of the input intensity S (W/cm^2) for $d=500$ μm (solid line), 250 μm (dashed line), and $d=150$ μm (dotted line). Here we take material parameters corresponding to MBBA, i.e., $\kappa=7.5\times10^{-12}N$, $n_0=1.54$, and $r=0.23$.

C. Quadratic beam profile

We conclude this section by the discussion of a last analytical case, the somewhat more realistic situation of a quadratic beam profile:

$$\beta(x)=\beta(1-4x^2/\Delta^2) \quad \text{for} \quad |x| \le \Delta/2$$
$$=0 \quad \text{otherwise} . \quad (4.24)$$

As before, we neglect the effects of diffraction and expand Eq. (2.7) to third order in θ and seek solutions of the form $\theta(x,z)=a(x)\sin(\pi z/d)$, with $a(x)$ governed by the diffusion equation (4.7). The symmetry of the pump intensity about $x=0$ suggests an expansion of $a(x)$ as

$$a(x)=a_0-a_2x^2+a_4x^4-\cdots . \quad (4.25)$$

We assume $a_2 \ll a_0$ and keep terms up to second power in x. This is consistent near the threshold of the Freedericksz transition. Inserting this ansatz into Eq. (4.7) yields

$$a_2=-\frac{a_0 r}{2}(\beta-\pi^2/d^2 r-3\beta\alpha a_0^2/4) . \quad (4.26)$$

At $|x|=\Delta/2$, the solution (4.25) and its derivative must go continuously into the solution (4.20) which reads now

$$a(x)=C\exp(-\pi|x|/d) . \quad (4.27)$$

These conditions allow to determine the constants a_0 and C. One finds for a_0 thc three possible values

$$a_0=0 , \quad (4.28a)$$

$$a_0=\pm\left[\frac{(\beta-\pi^2/d^2 r)(\Delta/2+\pi\Delta^2/8d)-\pi/dr}{3\beta\alpha\Delta(1+\pi\Delta/4d)/8}\right]^{1/2} , \quad (4.28b)$$

and for C

$$C=a_0 e^{\pi\Delta/2d}\left[1-\frac{\Delta^2 r}{8}(\beta-\pi^2/d^2 r-\tfrac{3}{4}\beta\alpha a_0^2)\right] . \quad (4.29)$$

A nonzero solution for a_0 is possible only if

$$\beta \ge \frac{\pi^2}{d^2 r}+\frac{8\pi}{\Delta r}(4d+\pi\Delta)^{-1} . \quad (4.30)$$

The first term on the right-hand side of Eq. (4.30) is the plane wave OFT threshold intensity (3.10). For r positive, which is the case here, the threshold intensity is larger in the case where the incident laser has a transverse profile.[18] The smaller the radius of the incident beam, the higher the threshold intensity of the OFT.

V. DYNAMICS

In order to analyze the stability and the dynamics of the solutions presented in the preceding sections, we introduce a phenomenological Debye-type relaxation of the director angle proportional to the viscosity of the liquid crystal.[12] This is a good approximation provided that thermal effects can be neglected. The equation of motion for the director-angle distribution now becomes [compare with Eq. (2.7)]

$$\partial_{xx}^2\theta(x,z,t)+\partial_{zz}^2\theta(x,z,t)+\beta(x)r\frac{\sin\theta\cos\theta}{(1-r\sin^2\theta)^{3/2}}=\frac{\gamma}{\kappa}\partial_t\theta(x,z,t)\ . \quad (5.1)$$

We first analyze the stability of the one-dimensional higher-order spatial modes of Sec. III in the limit of small anisotropy $r \ll 1$.

A. One-dimensional small-anisotropy model

In the one-dimensional small-anisotropy limit, Eq. (5.1) reduces to

$$\partial_{zz}^2\theta(z,t)+\beta r\sin\theta\cos\theta=\frac{\gamma}{\kappa}\partial_t\theta\ . \quad (5.2)$$

We use this equation to perform a linear stability analysis of the spatial modes of the director $\theta(z)$. To this end, we perturb the steady-state solution (3.5) by a small time-dependent quantity $\epsilon(z,t)$:

$$\theta(z,t)=\theta_{st}(z)+\epsilon(z,t)\ . \quad (5.3)$$

Introducing (5.3) into Eq. (5.2), factorizing $\epsilon(z,t)$ as $\epsilon(z,t)=A(z)e^{\Gamma t}$, and keeping only terms linear in ϵ, yields the eigenvalue equation

$$d_{zz}^2A+[g(z)-\lambda]A=0 \quad (5.4)$$

where $\lambda=\Gamma\gamma/\kappa$ and the potential $g(z)$ is

$$g(z)=\beta r\left[1-\frac{2}{\mu^2}\mathrm{sn}^2(\sqrt{\beta r}z)\right]\ . \quad (5.5)$$

The stability of $\theta_{st}(z)$ against small perturbations is determined by the sign of the maximum eigenvalue λ_{max}, which must be negative for the steady-state solution to be stable.

We proceed by expanding $A(z)$ on the complete and orthogonal basis of $\{\sin(n\pi z/d)\}$, n integer. The eigenvalues λ_n are then obtained by diagonalizing the matrix L of elements

$$L_{nm}=\frac{2}{d}\int_0^d dz\left[\sin\left[\frac{n\pi z}{d}\right][\partial_{zz}^2+g(z)]\sin\left[\frac{m\pi z}{d}\right]\right]\ . \quad (5.6)$$

A numerical diagonalization of L shows that for the lowest-order spatial mode, λ_{max} is always negative, starting at 0 for $\beta=\beta_{th}^1$ and decreasing monotonically for increasing β. This proves the stability of the first mode against small perturbations above the OFT threshold.

In contrast, the linear stability analysis around the second and higher sn modes shows these to be unstable. In these cases, λ_{max} is positive for $\beta=\beta_{th}^m$, and decreases monotonically for increasing β, to asymptotically reach 0 as $\beta\to\infty$. This is illustrated in Fig. 6 for the case of the second spatial mode $m=2$.

We have studied numerically the dynamical evolution (5.2) of the directors by discretizing the problem along the longitudinal dimension, using a three-point evaluation of the second-order spatial derivative. This reduces the problem to the solution of a system of coupled first-order differential equations in time. The boundary conditions $\theta(z=0,t)=\theta(z=d,t)=0$ were used to evaluate the second derivatives at the surfaces of the sample. Typical results of this analysis are presented in Fig. 7. The following general trends are observed.

If the system is initially close to the unstable homogeneous mode $\theta(z)=0$ and irradiated with a laser of intensity $\beta>\beta_{th}^1$, the directors evolve in time towards a spatial distribution corresponding to the first sn mode in a time inversely proportional to $(\beta-\beta_{th}^1)$. (Note that the details of our numerical algorithm imposed that the director angle takes positive values in this case. The stochastic description of Sec. VII shows that in fact the evolution to a physically equivalent negative θ distribution is just as likely.) This evolution, illustrated in Fig. 7(a), is confirmed by a linearized determination of the switch-on

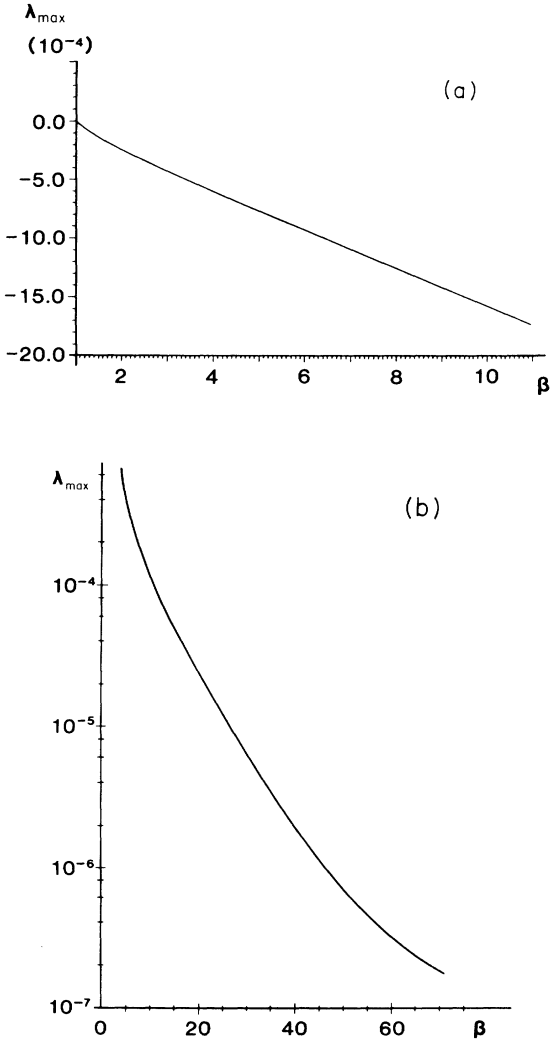

FIG. 6. Maximum eigenvalue λ_{max} as a function of β, for (a) the first and (b) the second sn mode. The eigenvalues were calculated using eight sine functions in the first case and 32 in the second. In both cases a further increase of the number of basis functions left the eigenvalues unchanged.

time τ_{on}, which gives

$$\tau_{on}=\left[\frac{\kappa}{\gamma}\frac{\pi^2}{d^2}\left[\frac{\beta-\beta_{th}^{l}}{\beta_{th}^{l}}\right]\right]^{-1} . \tag{5.7}$$

Equation (5.7) displays critical slowing down around the threshold condition $\beta\cong\beta_{th}^{l}$, which is again indicative of a phase transition.

This same first-order mode is also reached if the system is initially close to a higher-order spatial mode [Fig. 7(b)], confirming the fact that they are unstable. However, the lifetime of these modes becomes very long for high enough incident intensities, as already seen in Fig. 6. In practice, this means that high incident intensities can be used to trap the system in the vicinity of the higher-order longitudinal modes for very long times [minutes or hours for 4-methoxybenzylidene-4-(*n*-butyl)aniline (MBBA)]. Note however that these higher modes cannot be reached by a continuous change of β from $\beta\leq\beta_{th}^{m}$, but could be present in transient situations where the system is abruptly driven into a new regime (hard-mode excitation) or in resonator configurations. Furthermore, these higher-order modes will show up in the statistical mechanics of the problem, although this aspect is not considered here.

B. Two-dimensional problem, small-θ expansion

Let us now turn to the more realistic two-dimensional description of the system. In the case of weak plane-wave illumination, the stability analysis of the steady-state solutions can be performed analytically by developing the nonlinearity in Eq. (5.1) to third order in θ, and seeking a solution of the type $\theta(x,z,t)=a(x,t)\sin(\pi z/d)$. The resulting equation of motion for $a(x,t)$ is the nonlinear diffusion equation

$$\frac{\gamma}{\kappa}\partial_t a(x,t)-\partial_{xx}^2 a(x,t)$$
$$=(\beta r-\pi^2/d^2)a(x,t)-\tfrac{3}{4}\alpha\beta r a^3(x,t) . \tag{5.8}$$

Linearizing $a(x,t)$ about the steady state $a_{st}(x)$ [Eq. (4.15)]

$$a(x,t)=a_{st}(x)+\epsilon(x,t) \tag{5.9}$$

and factorizing the small perturbation $\epsilon(x,t)$ as $A(x)\exp(\Gamma t)$, yields

$$d_{xx}^2 A+(\beta r-\pi^2/d^2-\tfrac{9}{4}\alpha\beta r a_{st}^2-\gamma\Gamma/\kappa)A=0 . \tag{5.10}$$

The stability of the inhomogeneous steady-state solution (4.15) is obtained by substituting its value into (5.10). Introducing

$$\begin{aligned} y&=x+C_1/\nu ,\\ \nu&=[\tfrac{1}{2}(\beta r-\pi^2/d^2)]^{1/2} ,\\ \mu&=3(\beta r-\pi^2/d^2) ,\\ \Omega&=-2(\beta r-\pi^2/d^2)-\gamma/\kappa\Gamma , \end{aligned} \tag{5.11}$$

we obtain the eigenvalue equation

$$d_{yy}^2 A(y)+\left[\Omega+\frac{\mu}{\cosh^2(\nu y)}\right]A(y)=0 . \tag{5.12}$$

Its eigenvalues Ω_n are well known[19] and imply, with (5.11)

$$\Gamma_n=-(\kappa/2\gamma)(\beta r-\pi^2/d^2)n(4-n) , \tag{5.13}$$

together with the condition

$$\Gamma_n\leq(\kappa/\gamma)(\beta r-\pi^2/d^2) , \tag{5.14}$$

which limits the possible values of n to $n\leq 4$. For these values, Γ_n is always negative for $\beta\geq\beta_{th}$, that is, the inhomogeneous steady-state solution is stable. This demonstrates the possibility of inducing a stable inhomogeneous transverse distribution of directors under homogeneous plane-wave pumping.

Nonlinear diffusion equations of the form (5.8) have been studied in considerable detail in biology, where they describe selection-migration processes. They are known[20,21] to sustain traveling-wave solutions of the form $a(x,t)=a(x-vt)$. In our specific case, we obtain three generic types of wave fronts, all others being obtained by translation and parity inversion. Taking a_∞ with the + sign in (4.11), they can be expressed as

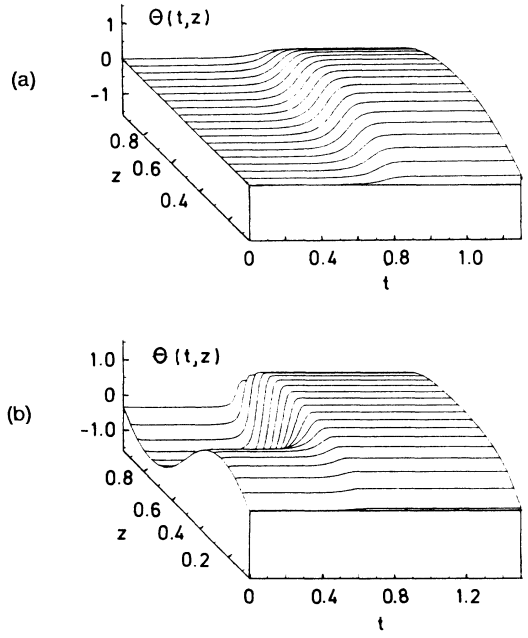

FIG. 7. Dynamical evolution of $\theta(z,t)$ towards the first sn mode for $d=250$ μm, the crystal parameters of Fig. 6, and $\gamma=0.8$ P; (a) $\theta(z,t)$ evolving from a very small homogeneous initial angle distribution $\theta(z,t=0)=10^{-5}$, for $\beta=2$; (b) same for an initial distirbution $\theta(z,t=0)=\sin(2\pi z/d)$ and $\beta=6$.

$$a_{12}(x,t)=\tfrac{1}{2}a_\infty\left\{-1+\tanh\left[\frac{\rho a_\infty}{4}\left[x+\frac{3}{2}\frac{\kappa}{\gamma}\rho a_\infty t\right]\right]\right\},$$
$$a_{13}(x,t)=a_\infty\tanh(\sqrt{\tfrac{3}{8}\alpha\beta r}\,a_\infty x)\,, \tag{5.15}$$
$$a_{23}(x,t)=\tfrac{1}{2}a_\infty\left\{1+\tanh\left[\frac{\rho a_\infty}{4}\left[x+\frac{3}{2}\frac{\kappa}{\gamma}\rho a_\infty t\right]\right]\right\},$$

where $\rho=\sqrt{3\alpha\beta r/2}$.

The wave front a_{13} that links the two stable solutions $\pm a_\infty$ is stationary. The other two, which connect the unstable solution $a=0$ to one of the stable ones, propagate at the intensity-dependent velocity

$$v=\frac{3}{2}\frac{\kappa}{\gamma}\rho a_\infty\,, \tag{5.16}$$

to bring the whole crystal to a stable homogeneous configuration. It has been conjectured by Fife[21] that the traveling-wave solutions (5.15) are the only stable solutions of the nonlinear diffusion equation (5.8).

VI. NUMERICAL STUDY OF THE FULL NONLINEAR MODEL

This section presents results of a numerical analysis of the two-dimensional OFT in the case of an incident laser with Gaussian intensity profile, and including the full nonlinearity. As before, we assume a single elastic constant and neglect the effects of diffraction.

In steady state, this situation is described by Eq. (2.7) with a Gaussian transverse dependence of $\beta(x)$:

$$\beta(x)=\beta_0\exp(-x^2/\omega_0^2)\,, \tag{6.1}$$

where ω_0 is the beam diameter.

To solve this equation numerically, we discretize the problem in x, using a three-point algorithm to evaluate the second-order spatial derivative with respect to x. The transverse domain of integration $-x_{\max}\le x\le x_{\max}$ is taken to be broad compared to the spot size ($x_{\max}\gg\omega_0$) so that we can make the assumption $\theta_{j-1}=0$ in the first step of integration and $\theta_{j+1}=0$ in the last one. We obtain a system of second-order differential equations, with fixed boundary conditions

$$\theta(x,z=0)=\theta(x,z=d)=0,$$
$$\theta(x_{\max+1},z)=\theta(-x_{\max+1},z)=0\,. \tag{6.2}$$

that can be integrated with respect to z.

Figure 8 illustrates the steady-state spatial structure of the director angle $\theta(x,z)$ for two values of the peak pump intensity β_0 above the plane-wave OFT threshold $\beta_{\rm th}^1$. For $\beta_0=1.92\beta_{\rm th}^1$ [Fig. 8(a)], the solution is in the form of a "1_z1_x" mode that corresponds to the first z mode, with a maximum angle of reorientation in the middle of the sample, and the first x mode, with a maximum angle at $x=0$. As β_0 is increased, higher modes become possible, such as the 1_z3_x mode illustrated in Fig. 8(b) for $\beta_0=8.86\beta_{\rm th}^1$. Even higher modes can be reached if the input intensity is further increased.

The main results of a systematic numerical experiment are summarized in Fig. 9. The solid line shows the peak

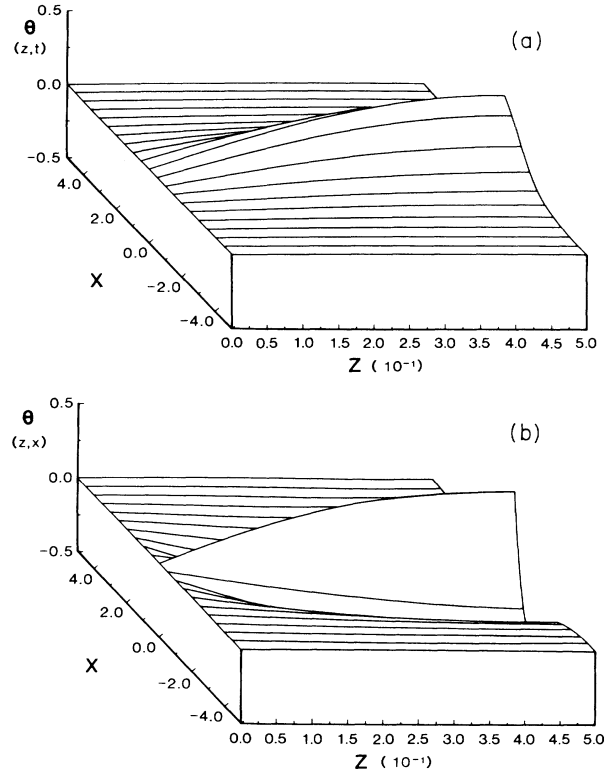

FIG. 8. Steady-state spatial distribution $\theta(z,x)$ for a sample length $d=250$ μm and a Gaussian input beam of waist $\omega_0=100$ μm; (a) 1_z1_x mode for $\beta=1.92$; (b) 1_z3_x mode for $\beta=8.86$. (z and x are scaled to d and ω_0, respectively). Crystal parameters of Fig. 6.

threshold intensity $\beta_{0,\rm th}$ for the onset of the 1_z1_x mode as a function of the beam-waist ω_0. $\beta_{0,\rm th}$ decreases with increasing ω_0, and converges as expected to the plane-wave threshold $\beta_{\rm th}^1$ for $\omega_0\to\infty$. In contrast, the integrated flux over the Gaussian profile is as expected an increasing linear function of the beam diameter. These results, ob-

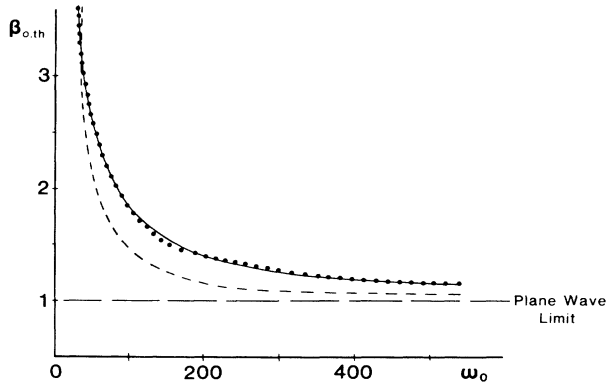

FIG. 9. Threshold peak intensity $\beta_{0,\rm th}$ for the onset of the lowest-order mode as a function of the spot size ω_0 (μm), for $d=250$ μm for three different beam profiles: Gaussian (solid line), quadratic (dashed line) and sech^2 (dotted line). Parameters of Fig. 6.

tained by a numerical integration of Eq. (2.7) with the form (6.1) of the incident intensity, is in good agreement with an analytical determination of the threshold based on a linearized version of (2.7) for small angles and using a $\mathrm{sech}^2(x/\omega_0)$ beam profile, which yields the result

$$\beta_{0,\mathrm{th}}=\beta_{\mathrm{th}}^{1}\left[1+\frac{1}{\pi(\omega_0/d)}\right]. \tag{6.3}$$

The dashed and dotted lines in Fig. 9 compare the value of the two-dimensional OFT threshold intensities obtained for quadratic [Eq. (4.30)] and sech^2 [Eq. (6.3)] beam profiles to the numerical values obtained for a Gaussian. All cases exhibit the same trends, but the quadratic beam profile shows too abrupt a decrease in $\beta_{0,\mathrm{th}}$ for increasing ω_0.

For the fundamental mode, the maximum angle of reorientation $\theta_{\max}$ is reached at the center of the sample, where the boundary conditions are the less strongly felt. This angle is bounded by $\pi/2$, which corresponds to the situation where the molecules are totally aligned with the field polarization in the middle of the sample. Figure 10 shows $\theta_{\max}$ as a function of β_0 for three values ω_0 of the spot size: for a given intensity β, $\theta_{\max}$ is larger, the broader the input beam, consistently with the fact that the OFT threshold decreases for increasing ω_0.

The dynamics of the system is obtained by numerically solving Eq. (5.1) for the Gaussian beam profile (6.1). Our numerical study indicates that the 1_z1_x mode is the only stable one. This is illustrated in Fig. 11 which depicts the evolution of the system initially in the 1_z3_x mode. As was the case for the plane-wave one-dimensional longitudinal modes, the higher-order modes can however have extremely long lifetimes if the crystal is irradiated by an intense laser beam, as will be discussed in more detail in Sec. VII. Switching between various modes can be induced by changing the peak incident power β_0 for a constant beam waist ω_0, but also ω_0 for constant β_0, as directly implied by the results of Fig. 9.

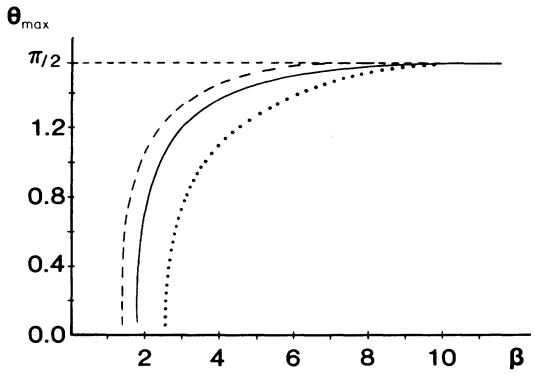

FIG. 10. Maximum reorientation angle $\theta_{\max}$ as a function of the scaled input intensity for various spot sizes and $d=250$ μm: $\omega_0=200$ μm (dashed line), $\omega_0=100$ μm (solid line), and $\omega_0=50$ μm (dotted line).

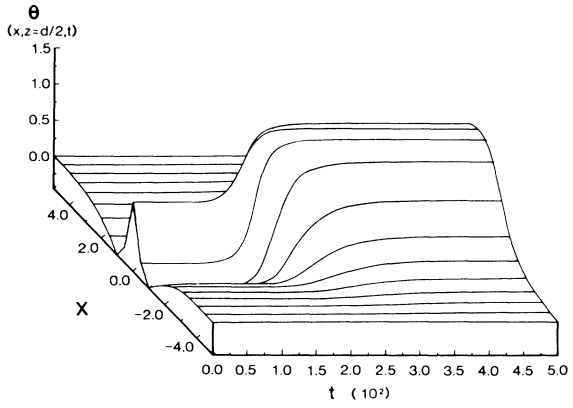

FIG. 11. Dynamical evolution of the 1_z3_x mode (same parameters as Fig. 8).

VII. STOCHASTIC DESCRIPTION

So far, we have treated the dynamics of the optical Freedericksz transition in a completely deterministic way. The analysis of Sec. V predicts that the system is invariably driven into the potential corresponding to the fundamental mode. To determine if this remains true in a real system in the presence of internal fluctuations, or whether it is only a feature of the deterministic model, we now introduce internal fluctuations in the medium and describe the transition as a stochastic process.

Specifically, we proceed by including internal fluctuations of the molecular alignment due to thermal agitation. We restrict our analysis to the simple model of a one-dimensional system and study specifically the transient dynamics of the director orientation when the laser is switched on. A similar case was discussed by Sagues and San Miguel,[22] who studied a stochastic model of the one-dimensional Freedericksz transition in a static magnetic field. They described the internal fluctuations of the liquid crystal by an additive noise term and the random fluctuations of the magnetic field by a multiplicative noise component. But their analysis was limited to third order in the reorientation angle θ, thus limiting its validity to low intensities of the magnetic field. Because of their multiplicative character, the fluctuations of the magnetic field shift the position of the minima of the potential, and hence the position of the threshold of the Freedericksz transition, the critical value of the field being reduced by a quantity proportional to the strength of correlations of the fluctuations of the magnetic field.

In contrast to this work we consider internal fluctuations only, but keep the nonlinearity to all orders in θ. This allows us to study the dynamics of higher-order modes. We discuss the case of a plane-wave incident laser field illuminating at normal incidence a homeotropically aligned sample of a nematic liquid crystal (NLC) of longitudinal dimension d and infinite transverse dimensions. The input laser beam is polarized along the x direction; we assume that the system is stable against fluctuations in the x-y plane, i.e., only fluctuations in the x-z plane are

amplified. The problem is then homogeneous in the transverse dimensions and reduced to a one-dimensional solution, where only the spatial longitudinal coordinate z is relevant.

The dynamics of the molecular reorientation angle $\theta(z,t)$ is then governed by the Langevin equation

$$\partial_t\theta=\frac{\kappa}{\gamma}\left[\partial_{zz}^2\theta+\beta r\frac{\sin\theta\cos\theta}{(1-r\sin^2\theta)^{3/2}}\right]+\eta(z,t)\ , \tag{7.1}$$

where a stochastic force η has been added to the one-dimensional form of the deterministic equation (5.1). We assume that the Langevin force $\eta(z,t)$ describes Gaussian white noise of zero mean and δ-function correlated,

$$\langle\eta(z,t)\eta(z',t')\rangle=2\varepsilon\delta(t-t')\delta(z-z')\ . \tag{7.2}$$

where ε is a constant which measures the strength of the fluctuations.

The deterministic part on the right-hand side of (7.1) corresponds to the variation of the free-energy density in the sample as the director angle θ is varied. This is easily seen by expressing the free energy $F(\theta)$ for this specific case as

$$\begin{aligned}F(\theta)&=A\int dz\,\mathcal{F}(\theta)\\&=A\int dz\tfrac{1}{2}\kappa[(\partial_z\theta)^2-2\beta(1-r\sin^2\theta)^{-1/2}]\ ,\end{aligned} \tag{7.3}$$

where A is the transverse area of the liquid-crystal sample. Defining the quantity $\delta\mathcal{F}/\delta\theta$ in a variational sense as

$$\frac{\delta\mathcal{F}}{\delta\theta}=\frac{\partial\mathcal{F}}{\partial\theta}-\frac{d}{dz}\frac{\partial\mathcal{F}}{\partial(\partial_z\theta)}\ , \tag{7.4}$$

allows to reexpress (7.1) as

$$\frac{\partial\theta}{\partial t}=-\frac{1}{A\gamma}\frac{\delta\mathcal{F}}{\delta\theta}+\eta(z,t)\ , \tag{7.5}$$

as advertised.

An equivalent way to proceed is by means of the Fokker-Planck equation associated to the Langevin equation (7.1). This equation governs the transition probability to a specified state characterized by a given $\theta(z)$ distribution from an initial state $\theta_0(z)$. The Fokker-Planck equation is a dynamical equation for this probability $W(\theta)$, given an initial condition θ_0. The Fokker-Planck equation associated to the Langevin equation (7.1) is

$$\partial_t W(\theta)=-\partial_\theta[h(z,t)W(\theta)]+\partial_{\theta\theta}^2[g(z,t)W(\theta)]\ , \tag{7.6}$$

where

$$\begin{aligned}h(z,t)=&\lim_{\tau\to0}\frac{1}{\tau}\langle\theta(t+\tau)-\theta(t)\rangle\\&\times\frac{\kappa}{\gamma}\left[\partial_{zz}^2\theta+\beta r\frac{\sin\theta\cos\theta}{(1-r\sin^2\theta)^{3/2}}\right]\ ,\end{aligned} \tag{7.7}$$

and

$$g(z,t)=\tfrac{1}{2}\lim_{\tau\to0}\frac{1}{\tau}\langle[\theta(t+\tau)-\theta(t)]^2\rangle=\varepsilon\ . \tag{7.8}$$

The stationary solution $W_{\rm st}(\theta)$ of (7.6) is given by

$$W_{\rm st}(\theta)=\mathcal{N}\exp\left[-\frac{F(\theta)}{kT}\right]\ , \tag{7.9}$$

where k is the Boltzmann constant, T the temperature in K, and $\mathcal{N}$ a normalization constant. In steady state, the most probable molecular configuration corresponds to a minimum of the free energy.

A. Langevin approach—numerical solution

This section studies the transition from the uniform homeotropic orientation to a nonuniform θ distribution by solving numerically Eq. (7.1) for a large number of realizations of the noise force η. This allows us to discuss the effects of fluctuations on the behavior of the system in a statistical sense. In particular, the characteristic average time for the onset of a nonhomogeneous molecular distribution is determined by averaging the result of computer simulations of the stochastic process over a large number of realizations.

In a series of numerical experiments, we have switched the laser at time $t=0$ from zero to a fixed intensity larger than threshold. The initial molecular orientation is homogeneous and characterized by $\theta(z,t=0)=0$. The time evolution of θ is followed during 100 sec. After the laser is switched on, the internal fluctuations start being amplified and drive the system away from the now unstable homogeneous initial state into a nonhomogeneous distribution (Freedericksz transition). Averaging over all realizations allows us to determine the statistics of the switch-on time τ for the onset of a nonhomogeneous reorientation distribution.

The first series of realization of the stochastic process was performed for a constant laser intensity β equal to ten times the plane-wave threshold of the OFT. The most remarkable result is that the second spatial mode was reached, in a few cases, in contrast to the deterministic case. This second mode is very close to the second mode of the elliptic sine function, which is the approximate solution obtained in Sec. II for the case of small dielectric anisotropy. (In the numerical calculations performed here, the dielectric anisotropy r was fixed to $r=0.23$, corresponding to MBBA.) In some cases the system was found to evolve towards the second longitudinal mode and to sustain this reorientation distribution for times in excess of 100 sec.

Several examples of the dynamics of $\theta(z,t)$ are illustrated in Fig. 12 for $D=\varepsilon/d=10^{-4}$. Case (a) corresponds to the most commonly found dynamical evolution of θ: the unstable zero solution evolves towards the fundamental inhomogeneous longitudinal mode, where saturation occurs in the reorientation (a large part of the longitudinal profile of θ reaches the maximum value $\pm\pi/2$). The sign of θ is of course physically irrelevant, i.e., $\theta(z,t)$ is physically equivalent to $-\theta(z,t)$. Positive and negative angles of reorientation have been observed to appear with equal frequencies within the statistical uncertainty of our numerical experiment.

Case (b) represents the situation already mentioned where the fluctuations drive the system into the second

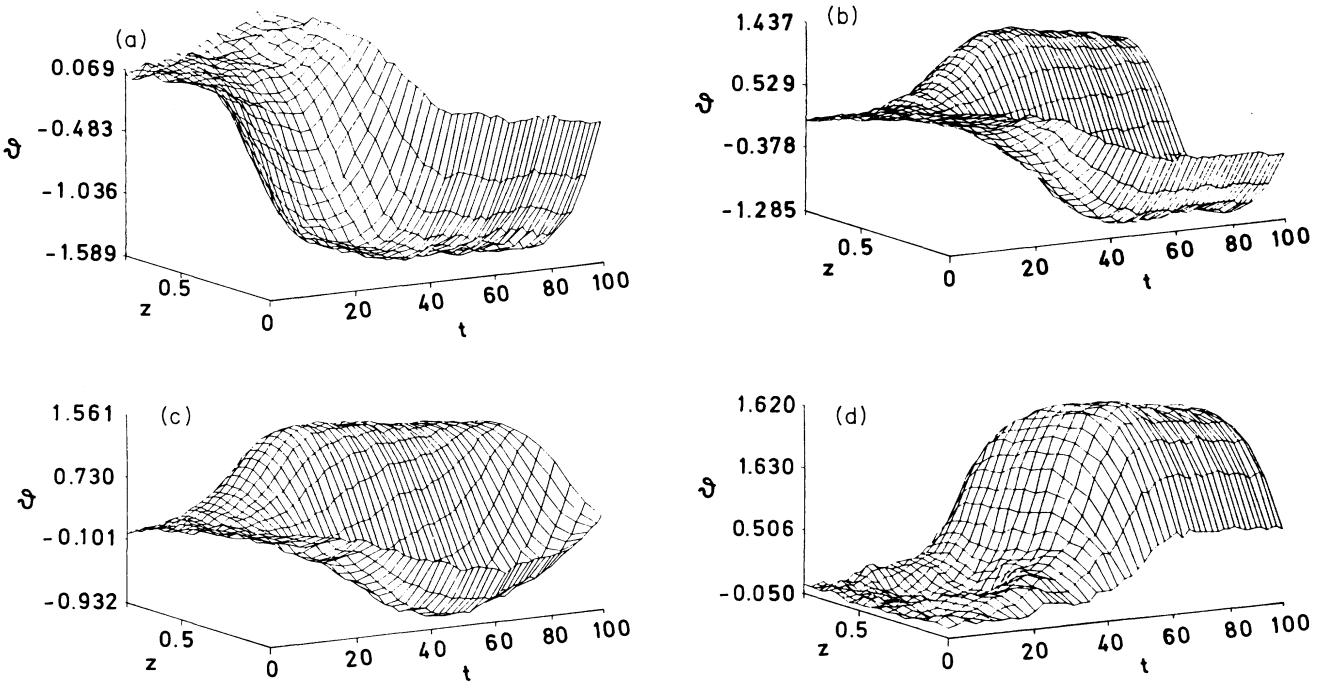

FIG. 12. Examples of the dynamical behavior of $\theta(z,t)$ for $D=10^{-4}$, $d=250$ μm, and $\beta=10\beta_{\text{th}}$.

spatial mode. The longitudinal profile at time $t=100$ sec is not always as perfectly symmetric as would be expected from the deterministic model, suggesting that for those specific realizations, the second mode is only a transient solution and that for longer integration times, the fluctuations will drive the system back into the fundamental mode. Such a situation is illustrated in Fig. 12(c), where the second mode is clearly excited in a transient regime before the fundamental distribution is reached. Still, it is interesting to see that contrary to what might be expected in view of the deterministic analysis, the OFT can in principle lead to higher modes of the molecular orientational distribution than the fundamental one.

With an input intensity ten times above threshold, the third mode of reorientation can in principle be reached. In the 200 realizations studied in this experiment, the third mode never appeared clearly, but in a few cases, the very first part of the evolution showed a tendency to evolve towards such a mode. In the case reproduced in Fig. 12(d), the longitudinal profile is characterized for short times by two minima, one on each side of $z=d/2$, typical of a third-order mode reorientation. This profile is however rapidly washed out and the clear evolution towards the fundamental mode takes place.

To determine the switch-on time τ_m to the mth nonhomogeneous reorientation, we note that for a fixed input intensity β and away from saturation, the maximum reorientation angle $\theta_{\max,m}$ and its position z_m are different for each mode m (see Sec. III). We thus define τ_m (somewhat arbitrarily) as the time after which $\theta(z_m,t)$ reaches the value $\frac{1}{2}\theta_{\max,m}$ at z_m.

Averaging the values of τ_m over all realizations of the stochastic process allows to determine the statistics of the switch-on times to the different modes. Figure 13 summarizes results for $\beta=10\beta_{\text{th}}$, $D=10^{-4}$, and 200 realizations of the stochastic process. Histogram (a) is constructed from the 194 events that lead to the fundamental mode. The mean value of τ_1 is $\langle\tau_1\rangle=34.45$ sec, with a dispersion $\Delta=[(1/N)\langle(\tau_1-\langle\tau_1\rangle)^2\rangle]^{1/2}=8.19$ sec.

To analyze the effect of the noise strength on τ_1, a second series of 200 realizations was integrated for the smaller noise strength $D=10^{-5}$. The results of the 194 realizations leading to the fundamental mode are reported in Fig. 13(b). We now have $\langle\tau_1\rangle=44.61$ sec and $\Delta=8.56$ sec; as expected, for smaller noise the system needs a longer time to escape the unstable homogeneous state $\theta(z)=0$. Reducing D by a further factor of 10 to $D=10^{-6}$ leads to a still increased value of the switch-on time, $\langle\tau_1\rangle=51.73$ sec and $\Delta=8.72$ sec.

A similar numerical experiment was performed for $D=10^{-4}$ and $\beta=20\beta_{\text{th}}$. In this case, higher-order modes are expected to be reached with a higher frequency. We found indeed that out of 200 realizations of the stochastic process, 160 corresponded to a Freedericksz transition to the fundamental inhomogeneous mode, the 40 remaining cases leading to the second mode. In this case $\langle\tau_1\rangle=16.87$ sec, with the significantly weaker dispersion $\Delta=3.09$ sec [see Fig. 13(c)].

Comparing this series of realizations to the results $\beta=10\beta_{\text{th}}$ shows that for a given noise strength, it is much more probable to see a Freedericksz transition to a higher mode when the intensity of the laser is large, and the first

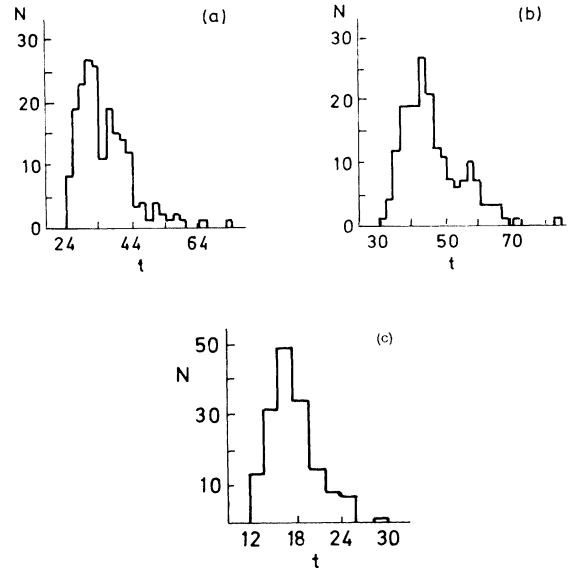

FIG. 13. Distribution of switch-on times τ_1 to the first nonhomogeneous mode of the reorientation. Each histogram is constructed from a series of 200 realizations of the stochastic noise. Time in seconds. (a) $\beta=10\beta_{th}$, $D=10^{-4}$; (b) $\beta=10\beta_{th}$, $D=10^{-5}$; (c) $\beta=20\beta_{th}$, $D=10^{-4}$. Note the different time scales on the histograms.

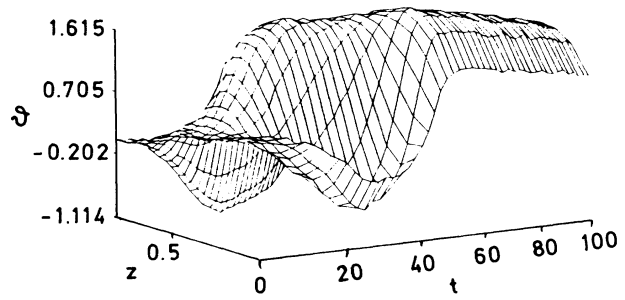

FIG. 14. Example of the dynamics of the Freedericksz transition for $\beta=20\beta_{th}$. The noise strength is $D=10^{-4}$.

part of the evolution is characterized by a richer structure. The number of realizations for which an evolution towards a higher mode (third or even fourth) shortly appears in a transient regime is increased with the intensity. For example, the realization of Fig. 14 clearly displays a transient evolution from the unstable zero state to the third mode, with a final evolution towards the fundamental distribution.

B. Fokker-Planck approach

Section VII A showed that under the influence of internal fluctuations, a Freedericksz transition can be induced not only to the fundamental nonhomogeneous state, but also, at least in a transient, to several higher modes. We now present a probabilistic, Fokker-Planck description of the steady-state statistical distribution of the possible orientational states $\theta(z,t)$. Equation (7.9) shows that in steady state, the free energy plays the role of the generalized potential $U(\theta)$. The statistical distribution of the different modes can then be directly deduced from the variations of F as the input intensity is increased above threshold. Absolute probabilities cannot be determined, but ratios between probabilities to observe a given asymptotic state can be worked out by comparing the free energy of the liquid crystal in these states.

To illustrate this point, we return to the simplified model of a small dielectric anisotropy of Sec. III. In this limit the different deterministic distributions of θ are given in steady state by the successive modes (3.6) of the elliptic sine function, and the free energy becomes

$$F=A\kappa\beta\int_0^d dz\left[\frac{r}{2}\frac{1}{\mu^2[1-1/\mu^2\mathrm{sn}^2(\sqrt{\beta r}z)]}\mathrm{cn}^2(\sqrt{\beta r}z)dn^2(\sqrt{\beta r}z)-\left[1-\frac{r}{\mu^2}\mathrm{sn}^2(\sqrt{\beta r}z)\right]^{-1/2}\right], \tag{7.10}$$

where $1/\mu$ is the modulus of the elliptic functions. The functions $\mathrm{cn}(u,1/\mu)$ and $\mathrm{dn}(u,1/\mu)$ can be related to the Jacobian elliptic sine function through the relations[23]

$$\mathrm{cn}^2(u,1/\mu)=1-\mathrm{sn}^2(u,1/\mu)$$

and

$$\mathrm{dn}^2(u,1/\mu)=1-1/\mu\mathrm{sn}^2(u,1/\mu)\ .$$

For intensities below threshold, the free energy is simply expressed by the linear relation $F=-\kappa\beta d$.

Performing the integral numerically for β above threshold yields a negative free energy that is a decreasing function of the input intensity: the potential minimum becomes deeper as β is increased. The negative sign is because the electromagnetic energy overcomes the elastic energy above threshold. For a fixed intensity, F is more negative, the lower the index of the mode, implying that the fundamental mode of molecular reorientation is the most likely to appear asymptotically.

Each mode of molecular reorientation corresponds to a minimum of the free energy. It is deepest for the fundamental mode, and becomes increasingly shallower with the order of the mode. In other words, the higher modes are only transient solutions and evolve asymptotically towards the fundamental reorientation under the influence of noise. We introduce the short-hand notation $W(n)$ to denote the steady-state probability to find the nth mode of the molecular reorientation; the ratio of probabilities to observe a transition to two different modes n and m of the molecular reorientation is proportional to

$$\frac{W(n)}{W(m)}\cong\exp[-F(n)+F(m)]\ , \tag{7.11}$$

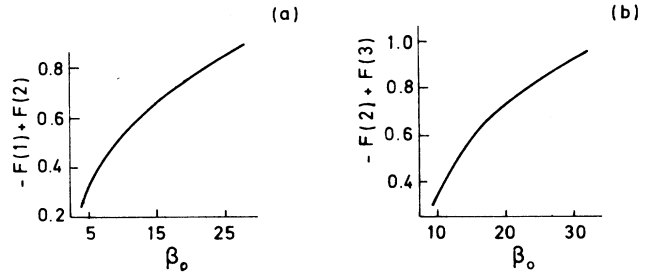

FIG. 15. Difference in free energies between (a) the second and first spatial modes and (b) the third and second spatial modes as a function of the pump intensity, in units of the threshold intensity β_{th}.

where $F(n)$ expresses in the same way the free energy of the liquid crystal in the nth mode of the molecular reorientation. The differences $-F(n)+F(m)$ are plotted in Fig. 15 for (a) the first two modes and (b) the second and third modes. These quantities are always positive, and increase for increasing values of the input field, confirming that the lowest-order mode is always the more probable to appear when a Freedericksz transition occurs.

VIII. SUMMARY AND CONCLUSION

We have investigated theoretically dynamical aspects of the optical Freedericksz transition in nematic liquid crystals, combining simplified analytical models and a numerical study of a full two-dimensional description. In one dimension, the crystal can exhibit higher-order spatial modes of very long lifetime that might be observed by hard-mode excitation. In the more realistic two-dimensional case, we have shown that due to the transverse correlations of the director angle, inhomogeneous transverse structures and traveling-wave type transverse propagation of the director angle field is possible even under plane-wave excitation. When the crystal is irradiated by a Gaussian beam, unstable mode structures are possible, but as in the one-dimensional case, they are unstable (but long lived), except for the fundamental. These results will be of practical importance in connection with the realization of spatial light modulators.

Our stochastic description of the Freedericksz transition shows clearly that higher-mode solutions can be reached in a transient regime. These appear in numerical simulations for high enough incident intensities of the laser, even if the fundamental mode is the most likely to appear asymptotically.

It will be interesting in subsequent work to introduce external fluctuations of the laser intensity[22] and to analyze the effects of the resulting colored noise on the optical Freedericksz transition. Future work will also include a generalization of the present results to a more realistic full three-dimensional geometry, including the full three-dimensional nucleation problem.

Note added in proof. The effect of fluctuations on domain walls near the Freedericksz transition has been recently discussed by W. Xiu Lu, Phys. Rev. A **34**, 5179 (1986).

ACKNOWLEDGMENTS

This research is supported by the National Science Foundation/Industry Optical Circuitry Cooperative. One of us (F.M.) acknowledges partial support by the Swiss National Fund for Scientific Research. The research of one of us (A.E.K.) is supported by the U.S. Air Force Office of Scientific Research. We are indebted to Professor Y. R. Shen for bringing the beauty of liquid-crystal physics to our attention, and J. Gea-Banacloche for useful discussions.

*Also at Max-Planck-Institut für Quantenoptik, D-8046 Garching, Federal Republic of Germany.

†Present address: Department of Electrical and Computer Engineering, Johns Hopkins University, Baltimore, MD 21218.

[1]B. Ya. Zel'dovich, N. F. Pilipetskii, A. V. Sukhov, and N. V. Tabiryan, Pis'ma Zh. Eksp. Teor. Fiz. **31**, 287 (1980) [JETP Lett. **31**, 263 (1980)].

[2]B. Ya. Zel'dovich, N. V. Tabiryan, and Yu. S. Chilingaryan, Zh. Eksp. Teor. Fiz. **81**, 72 (1981) [Sov. Phys.—JETP **54**, 32 (1981)].

[3]B. Ya. Zel'dovich and N. V. Tabiryan, Zh. Eksp. Teor. Fiz. **82**, 1126 (1982) [Sov. Phys.—JETP **55**, 656 (1982)].

[4]S. D. Durbin, S. M. Arakelian, and Y. R. Shen, Phys. Rev. Lett. **47**, 1411 (1981).

[5]A. S. Zolot'ko, V. F. Kitaeva, N. Kroo, N. N. Sobolev, and L. Csillag, Pis'ma Zh. Eksp. Teor. Fiz. **34**, 263 (1981) [JETP Lett. **34**, 250 (1981)].

[6]I. C. Khoo and Shu-Lu Zhuang, Appl. Phys. Lett. **37**, 3 (1980).

[7]I. C. Khoo, Phys. Rev. A **23**, 2077 (1981).

[8]S. D. Durbin, S. M. Arakelian, and Y. R. Shen, Opt. Lett. **7**, 145 (1982).

[9]A. S. Zolot'ko, V. F. Kitaeva, N. N. Sobolev, and A. P. Sukhorukov, Zh. Eksp. Teor. Fiz. **81**, 933 (1981) [Sov. Phys.—JETP **54**, 496 (1982)].

[10]I. C. Khoo, J. Y. Hou, R. Normandin, and V. C. Y. So, Phys. Rev. A **27**, 3251 (1983).

[11]Mi-Mee Cheung, S. D. Durbin, and Y. R. Shen, Opt. Lett. **8**, 39 (1983).

[12]H. L. Ong, Phys. Rev. A **28**, 2393 (1983).

[13]I. C. Khoo, P. Y. Yan, T. H. Liu, S. Shepard, and J. Y. Hou, Phys. Rev. A **29**, 2756 (1984).

[14]P. G. de Gennes, *The Physics of Liquid Crystals* (Clarendon, Oxford, 1975).

[15]B. Ya. Zel'dovich and N. V. Tabiryan, Zh. Eksp. Teor. Fiz. **79**, 2388 (1980) [Sov. Phys.—JETP **52**, 1210 (1980)].

[16]S. I. Ben-Abraham, Phys. Rev. A **14**, 1251 (1976).

[17]F. Brochard, J. Phys. (Paris) **33**, 607 (1972).

[18]L. Csillag, I. Janossy, V. F. Kitaeva, N. Kroo, and N. N. Sobolev, Mol. Cryst. Liq. Cryst. **84**, 125 (1982).

[19]L. Landau and E. Lifshitz, *Quantum Mechanics* (Pergamon, New York, 1977), p. 73.

[20]A. M. Albano, N. B. Abraham, and D. E. Chyba, Am. J. Phys. **52**, 161 (1984).

[21]P. C. Fife, *Mathematical Aspects of Reacting and Diffusing Systems* (Springer-Verlag, Berlin, 1970).

[22]F. Sagues and M. San Miguel, Phys. Rev. A **32**, 1843 (1985).

[23]P. F. Byrd and M. D. Friedman, *Handbook of Elliptic Integrals for Engineers and Physicists* (Springer-Verlag, Berlin, 1954).